Int. J. Heat Mass Transfer. Vol. 35, No. 3, pp. 623–633, 1992
Printed in Great Britain

0017–9310/92 $5.00+0.00
Pergamon Press plc

Heat transfer in an annulus between independently rotating tubes with turbulent axial flow†

H. PFITZER and H. BEER

Institut für Technische Thermodynamik, Technische Hochschule Darmstadt,
Petersenstraße 30, 6100 Darmstadt, Germany

Abstract—The effects of the rotating inner and outer tube on the turbulent fluid flow and heat transfer in a concentric annulus are examined experimentally and by analysis. In the experimental investigations the heat transfer rate in the hydrodynamic and thermal entrance region of the rotating annulus and the velocity and temperature profiles at the end of the test section were determined. The analytical study was performed for flow and heat transfer of a fully developed turbulent flow in a rotating annulus by applying a modified mixing length theory. To express increase or suppression of turbulence, due to the centrifugal forces in the fluid caused by tube rotation, the mixing length was modified by a function of the Richardson number. The theoretical results for fully developed flow are compared with the experimental findings at the axial position of 60 hydraulic diameters downstream of the entrance.

1. INTRODUCTION

FLUID FLOW and heat transfer in rotating channels have been of great interest for many years. Taylor [1] investigated the stability of the flow between two concentric rotating cylinders. He found regular toroidal vortices in the annular gap for rotational speeds of the inner cylinder above a critical value. These so-called Taylor vortices develop because of an instability of the laminar flow due to a strong decrease in centrifugal forces with increasing radius. In a closed annular gap with no axial throughflow and with a rotating inner tube, Taylor vortices will arise at Taylor numbers $Ta_{kr} \geqslant 41.2$

$$Ta = \frac{v_{\varphi 1}(r_2 - r_1)}{\nu} \sqrt{\left(\frac{s}{r_m}\right)}. \quad (1)$$

With the aid of a bifurcation analysis for $Re_z \to 0$, Chandrasekhar [2] found a stabilizing effect by an imposed axial flow. For small flow-rate Reynolds numbers Re_z, the critical Taylor number increases according to

$$Ta_{kr}(Re_z) = Ta_{kr}(Re_z = 0) + 26.5\, Re_z^2. \quad (2)$$

The combined axial and rotational flow in an annulus with a rotating inner cylinder was studied experimentally by Kaye and Elgar [3]. For flow-rate Reynolds numbers $Re_z < 2000$, four flow regimes were detected in an annular gap

laminar flow
laminar flow with Taylor vortices
turbulent flow
turbulent flow with Taylor vortices.

The changes in the structure of the vortices with increasing axial velocity were investigated by Gu and Fahidy [4] by visualization. At small axial flows the individual Taylor cells get inclined and partial overlapping begins to appear. With further increase in the axial flow rate, the cell structure degenerates progressively to a disorderly pattern. At high axial flow rates the Taylor cells are hardly detectable and the complete degeneration of Taylor vortices is assumed.

Kuzay [5] experimentally studied the turbulent flow and heat transfer in a concentric annulus between a stationary and uniformly heated outer tube and a rotating adiabatic inner tube. The rotation rate $N_1 = v_{\varphi 1}/\bar{v}_z$ was varied up to 2.8 in the flow-rate Reynolds number range $1.5 \times 10^4 < Re_z < 6.5 \times 10^4$. Imposing a rotation to the axial flow, he found that the wall temperature of the outer tube diminished and the radial temperature profiles at the end of the heated annular gap, with a length of 36 hydraulic diameters, appreciably flattened. With increasing rotation, the inner boundary temperature rises while the outer wall temperature drops sharply. Therefore, the Nusselt number of a mixed-mode flow increases with increasing rotational velocity of the inner tube.

This paper describes the effect of independently rotating the inner and outer tube of a concentric annulus on the velocity and temperature distribution and on the heat transfer to a fluid flowing inside the annular gap. While the experiments deal with the fluid flow and heat transfer in the hydrodynamic and thermal entrance region, the analytical study was performed for a fully developed turbulent flow through a rotating annulus by applying a modified mixing length theory. To express the increase or suppression of turbulence, due to centrifugal forces in the fluid caused by tube rotation, the mixing length was modified by a function of the Richardson number. To our knowledge these

† Dedicated to Professor Dr.-Ing. Dr.-Ing.e.h. Ulrich Grigull.

NOMENCLATURE

a	thermal diffusivity
c_p	specific heat at constant pressure
d_h	hydraulic diameter
L	length of rotating test section
l	hydrodynamic mixing length in rotating annulus
l_0	hydrodynamic mixing length in stationary annulus
N_1	rotation rate of inner tube
N_2	rotation rate of outer tube
Nu	Nusselt number
Nu_m	mean Nusselt number
Pr	Prandtl number
Pr_t	turbulent Prandtl number
$Pr_{t,\infty}$	turbulent Prandtl number far from the wall
p	pressure
$\dot{q}_r$	heat flux density in radial direction
Re_z	flow-rate Reynolds number
Re_φ	rotational Reynolds number
Ri	Richardson number
r	radial coordinate
r_1	radius of inner tube
r_2	radius of outer tube
s	gap width
T	time mean temperature
T'	temperature fluctuation
Ta	Taylor number
v_r, v_φ, v_z	time mean velocities in r, φ, z-directions
v'_r, v'_φ, v'_z	velocity fluctuations in r, φ, z-directions
$\bar{v}_z$	mean axial velocity over annular cross section
$\tilde{y}_1$	dimensionless radial distance from the inner wall
$\tilde{y}_2$	dimensionless radial distance from the outer wall
z	axial coordinate.

Greek symbols

α	heat transfer coefficient
β	constant
ε_τ	eddy viscosity of momentum
ε_q	eddy diffusivity of heat
η	dynamic viscosity
θ	dimensionless temperature
κ	radius ratio
λ	thermal conductivity
λ_R	friction factor
ν	kinematic viscosity
ρ	density
τ	shear stress
φ	tangential coordinate.

are the first investigations performed in an annulus between co-rotating and counter-rotating tubes with turbulent axial flow.

2. EXPERIMENTS

A schematic outline of the horizontally mounted experimental apparatus is shown in Fig. 1. The rotating and heated test section has a length of $L/d_h = 60.94$, with a radius ratio $r_1/r_2 = 0.8575$ and an outer tube i.d. of $D = 180$ mm. The outer tube is heated electrically with a thin heating foil by means of a slip ring arrangement. The inner tube is made of synthetic, low conductivity material to obtain adiabatic conditions and is coated with a very thin tin foil to minimize heat radiation. In order to measure the axial development of the wall temperatures, both tubes are instrumented with thermocouples. The thermoelectric voltages were transmitted from the inner rotating tube to the stationary instrumentation with the aid of slip rings and from the outer rotating tube by a telemetric device.

At the end of the heated and rotating section a cylindrical three-hole aerodynamic probe as well as a hotwire probe could be inserted into the annular gap through small holes and traversed in the radial direction, in order to obtain axial and tangential velocity profiles. Step motors rotate the probe automatically against the main flow direction of the fluid. Temperature profiles could be detected by a traversable thermocouple probe on the other side of the annular gap at the end of the rotating test section.

Air is supplied by a centrifugal blower which is arranged at the end of the test rig to avoid heating of the air outside the test section. The inlet consists of an air filter, honeycombs and two wire mesh screens. The inlet section has a non-rotating length of six hydraulic diameters ($d_h = 2(r_2 - r_1)$) with the same radius ratio as the rotating test section. Behind the heated test section a mixing chamber for measuring the exit bulk temperature, a downstream non-rotating pipe, a Venturi nozzle for measuring the flow rate and the centrifugal blower are arranged. Rotation of both tubes was accomplished by means of two variable speed d.c. motors and pulley drives. The drive mechanisms provided continuous variation of the rotational speed from 50 to 2000 r.p.m.

The flow-rate Reynolds number Re_z was varied in the range $3000 \leqslant Re_z = \bar{v}_z d_h/\nu \leqslant 30000$ up to rotational Reynolds numbers $Re_{\varphi 1} = v_{\varphi 1} d_h/\nu \leqslant 20000$ at the inner tube and $Re_{\varphi 2} = v_{\varphi 2} d_h/\nu \leqslant 30000$ at the outer tube. Heat transfer coefficients and Nusselt numbers were determined from measurements of the inlet and outlet air temperatures, the

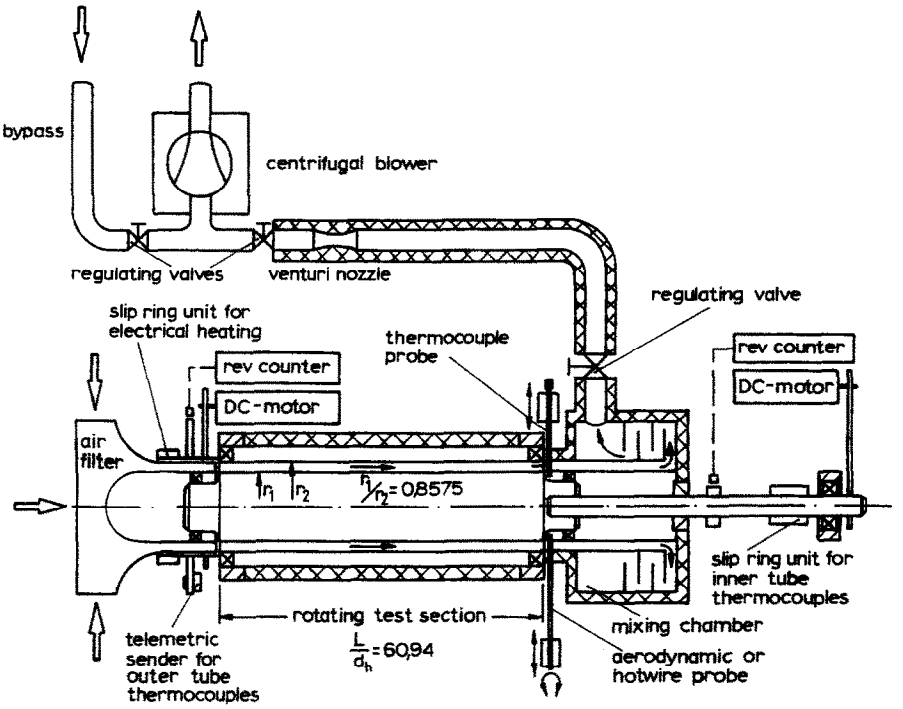

FIG. 1. Experimental apparatus.

wall temperatures of the outer heated tube and the mass flow.

3. ANALYSIS

In the theoretical investigation the governing time-averaged equations for mass conservation, the three momentum equations and finally the energy equation are solved after some simplifications for a fully developed and stationary flow of a Newtonian fluid. With this theoretical model the axial and tangential velocity profiles, the temperature profile, the friction factor and the Nusselt number for fully developed flow can be determined.

The following equations will be given in terms of a cylindrical coordinate system, with r, φ, z being the radial, tangential and axial coordinates. The corresponding time-averaged velocities are v_r, v_φ, v_z, the velocity fluctuations v_r', v_φ', v_z', the time-averaged temperature is T and the temperature fluctuations T'.

In stationary flow, with constant wall heat flux, all time derivatives become zero. Also, all derivatives in the axial direction become zero in a fully developed flow, except the constant pressure and temperature gradient. Additionally, there are no variations in the tangential direction, because of the axial symmetry of the system. With these simplifications and the assumptions of a negligible dissipation rate and no body forces, except the centrifugal force, the equations of conservation for an incompressible turbulent flow will take the form:

continuity equation

$$v_r = 0; \tag{3}$$

radial momentum equation

$$-\rho\frac{v_\varphi^2}{r} = -\frac{\partial p}{\partial r} + \frac{1}{r}\frac{\partial}{\partial r}(r\tau_{rr}) - \frac{1}{r}\tau_{\varphi\varphi}; \tag{4}$$

tangential momentum equation

$$0 = \frac{\partial}{\partial r}(r^2\tau_{r\varphi}); \tag{5}$$

axial momentum equation

$$0 = -\frac{\partial p}{\partial z} + \frac{1}{r}\frac{\partial}{\partial r}(r\tau_{rz}); \tag{6}$$

energy equation

$$\rho c_p v_z \frac{\partial T}{\partial z} = -\frac{1}{r}\frac{\partial}{\partial r}(r\dot{q}_r). \tag{7}$$

For a Newtonian fluid with constant properties the components of the stress tensor can be written as

$$\begin{aligned}
\tau_{rr} &= -\rho\overline{v_r'v_r'} \\
\tau_{\varphi\varphi} &= -\rho\overline{v_\varphi'v_\varphi'} \\
\tau_{r\varphi} &= \eta r\frac{\partial}{\partial r}\left(\frac{v_\varphi}{r}\right) - \rho\overline{v_r'v_\varphi'} \\
\tau_{rz} &= \eta\frac{\partial v_z}{\partial r} - \rho\overline{v_r'v_z'}.
\end{aligned} \tag{8}$$

The radial component of the heat flux vector is

$$\dot{q}_r = -\lambda\frac{\partial T}{\partial r} + \rho c_p \overline{v_r' T'}. \tag{9}$$

Because of the assumption of a fluid with constant properties, the equations of motion and the energy balance are uncoupled and will be solved separately, as shown in the following sections.

3.1. *The momentum equations*

For solving the momentum equations in the r, φ, z-directions the components of the turbulent Reynolds stress tensor must be replaced by new terms of a turbulence model. In this paper an eddy viscosity model has been used to calculate the turbulent Reynolds shear stresses

$$-\overline{v_r' v_z'} = \varepsilon_\tau \frac{\partial v_z}{\partial r}$$

$$-\overline{v_r' v_\varphi'} = \varepsilon_\tau r \frac{\partial}{\partial r}\left(\frac{v_\varphi}{r}\right). \tag{10}$$

Applying a modified Prandtl mixing length theory, the eddy viscosity can be written in the form

$$\varepsilon_\tau = l^2\left[\left(\frac{\partial v_z}{\partial r}\right)^2 + \left(r\frac{\partial}{\partial r}\left(\frac{v_\varphi}{r}\right)\right)^2\right]^{1/2} \tag{11}$$

as proposed by Koosinlin *et al.* [6]. The mixing length l is affected by the centrifugal force in a rotating system. For this reason Bradshaw [7] proposed the equation

$$\frac{l}{l_0} = \frac{1}{1+\beta Ri} \tag{12}$$

to modify the mixing length l_0 of a fluid in a non-rotating system with the dimensionless Richardson number Ri and the empirical constant β. A common correlation of the mixing length l_0 in a non-rotating straight duct is Nikuradse's mixing length expression [8], which is multiplied by van Driest's damping factor, in order to describe the disappearing mixing length near the wall in the viscous sublayer,

$$\frac{l_0}{r_2} = \frac{r_2 - r_1}{2r_2}\left[0.14 - 0.08\left(\frac{2r - r_2 - r_1}{r_2 - r_1}\right)^2 - 0.06\left(\frac{2r - r_2 - r_1}{r_2 - r_1}\right)^4\right]\left(1 - e^{-(\tilde{y}_1/26)}\right)\left(1 - e^{-(\tilde{y}_2/26)}\right). \tag{13}$$

In equation (13), $\tilde{y}_1$ and $\tilde{y}_2$ denote the dimensionless distances from the inner and outer wall of the annular duct:

$$\tilde{y}_1 = \frac{(r - r_1)v_*(r_1)}{\nu} = (r - r_1)\sqrt{\left(\frac{1}{\nu}\sqrt{\left(\left(\frac{\partial v_z}{\partial r}\bigg|_{r=r_1}\right)^2 + \left(r\frac{\partial}{\partial r}\left(\frac{v_\varphi}{r}\right)\bigg|_{r=r_1}\right)^2\right)}\right)}$$

$$\tilde{y}_2 = \frac{(r_2 - r)v_*(r_2)}{\nu} = (r_2 - r)\sqrt{\left(\frac{1}{\nu}\sqrt{\left(\left(\frac{\partial v_z}{\partial r}\bigg|_{r=r_2}\right)^2 + \left(r\frac{\partial}{\partial r}\left(\frac{v_\varphi}{r}\right)\bigg|_{r=r_2}\right)^2\right)}\right)} \tag{14}$$

where $v_*(r)$ is the friction velocity at the inner and outer wall. The Richardson number Ri is defined by

$$Ri = \frac{2\dfrac{v_\varphi}{r^2}\dfrac{\partial}{\partial r}(v_\varphi r)}{\left(\dfrac{\partial v_z}{\partial r}\right)^2 + \left(r\dfrac{\partial}{\partial r}\left(\dfrac{v_\varphi}{r}\right)\right)^2}. \tag{15}$$

In a fully turbulent straight duct flow without rotation, the Richardson number is equal to zero. In a rotating annular duct with radially growing tangential velocity, and therefore $Ri > 0$, the stabilizing effect of the centrifugal forces suppress the mixing length (see equation (12)). If the rotational speed of the inner tube is higher than that of the outer tube, Ri will become negative and the mixing length will increase. According to our experimental findings, the constant β is set to $\beta = 1$ for positive values of Ri and $\beta = 2.5$ for negative Richardson numbers.

After replacing the turbulent Reynolds stresses (equation (10)) by a function of the eddy viscosity (equation (11)) and after introducing the friction coefficient

$$\lambda_R = \frac{-\dfrac{\partial p}{\partial z}d_h}{\frac{1}{2}\rho\bar{v}_z^2}, \tag{16}$$

the momentum equation in the tangential direction will take the form

$$0 = \frac{\partial}{\partial r}\left((\nu + \varepsilon_\tau)r^3\frac{\partial}{\partial r}\left(\frac{v_\varphi}{r}\right)\right) \tag{17}$$

and in the axial direction it is

$$-\frac{\lambda_R \bar{v}_z^2}{2d_h} = \frac{1}{r}\frac{\partial}{\partial r}\left((\nu + \varepsilon_\tau)r\frac{\partial v_z}{\partial r}\right). \tag{18}$$

For the radial direction it can be shown that the radial pressure gradient is negligible as compared to the mean pressure in the duct.

For the numerical solution of the momentum equations the following dimensionless quantities are introduced:

radius

$$\tilde{r} = \frac{r}{r_2}$$

radius ratio

$$\kappa = \frac{r_1}{r_2};$$

length

$$\tilde{z} = \frac{z}{d_h} = \frac{z}{2r_2(1-\kappa)};$$

axial velocity

$$\tilde{v}_z = \frac{v_z}{\bar{v}_z};$$

tangential velocity

$$\tilde{v}_\varphi = \frac{v_\varphi}{\bar{v}_z};$$

flow-rate Reynolds number

$$Re_z = \frac{\bar{v}_z d_h}{\nu} = \frac{\bar{v}_z 2r_2(1-\kappa)}{\nu};$$

rotation rates

$$N_1 = \frac{v_{\varphi 1}}{\bar{v}_z}, \quad N_2 = \frac{v_{\varphi 2}}{\bar{v}_z};$$

eddy viscosity

$$\tilde{\varepsilon}_\tau = \frac{\varepsilon_\tau}{\nu};$$

mixing length

$$\tilde{l} = \frac{l}{r_2}. \tag{19}$$

Since the velocities $\tilde{v}_z$ and $\tilde{v}_\varphi$ are only functions of the radial coordinate $\tilde{r}$, the partial differentials are replaced by total differentials in the following equations. In the tangential momentum equation

$$0 = \frac{\mathrm{d}}{\mathrm{d}\tilde{r}}\left((1+\tilde{\varepsilon}_\tau)\tilde{r}^3 \frac{\mathrm{d}}{\mathrm{d}\tilde{r}}\left(\frac{\tilde{v}_\varphi}{\tilde{r}}\right)\right) \tag{20}$$

and in the axial momentum equation

$$-\frac{\lambda_R\, Re_z}{8(1-\kappa)^2} = \frac{1}{\tilde{r}}\frac{\mathrm{d}}{\mathrm{d}\tilde{r}}\left((1+\tilde{\varepsilon}_\tau)\tilde{r}\frac{\mathrm{d}\tilde{v}_z}{\mathrm{d}\tilde{r}}\right) \tag{21}$$

$\tilde{\varepsilon}_\tau$ denotes the dimensionless eddy viscosity

$$\tilde{\varepsilon}_\tau = \frac{Re_z}{2(1-\kappa)}\tilde{l}^2\sqrt{\left(\left(\frac{\mathrm{d}\tilde{v}_z}{\mathrm{d}\tilde{r}}\right)^2 + \left(\tilde{r}\frac{\mathrm{d}}{\mathrm{d}\tilde{r}}\left(\frac{\tilde{v}_\varphi}{\tilde{r}}\right)\right)^2\right)} \tag{22}$$

with the dimensionless mixing length

$$\tilde{l} = \frac{1-\kappa}{2}\left[0.14 - 0.08\left(\frac{2\tilde{r}-1-\kappa}{1-\kappa}\right)^2 - 0.06\left(\frac{2\tilde{r}-1-\kappa}{1-\kappa}\right)^4\right] \cdot \left(\frac{1}{1+\beta\, Ri}\right)\left(1-\mathrm{e}^{-(\tilde{y}_1/26)}\right)\left(1-\mathrm{e}^{-(\tilde{y}_2/26)}\right). \tag{23}$$

The Richardson number and the dimensionless distances from the inner and outer tube are defined as follows:

$$Ri = \frac{2\frac{\tilde{v}_\varphi}{\tilde{r}^2}\frac{\mathrm{d}}{\mathrm{d}\tilde{r}}(\tilde{v}_\varphi\tilde{r})}{\left(\frac{\mathrm{d}\tilde{v}_z}{\mathrm{d}\tilde{r}}\right)^2 + \left(r\frac{\mathrm{d}}{\mathrm{d}\tilde{r}}\left(\frac{\tilde{v}_\varphi}{\tilde{r}}\right)\right)^2} \tag{24}$$

$$\tilde{y}_1 = (\tilde{r}-\kappa)\sqrt{\left(\frac{Re_z}{2(1-\kappa)}\sqrt{\left(\left(\frac{\mathrm{d}\tilde{v}_z}{\mathrm{d}\tilde{r}}\right|_{\tilde{r}=\kappa}\right)^2 + \left(\tilde{r}\frac{\mathrm{d}}{\mathrm{d}\tilde{r}}\left(\frac{\tilde{v}_\varphi}{\tilde{r}}\right)\right|_{\tilde{r}=\kappa}\right)^2\right)}\right)}$$

$$\tilde{y}_2 = (1-\tilde{r})\sqrt{\left(\frac{Re_z}{2(1-\kappa)}\sqrt{\left(\left(\frac{\mathrm{d}\tilde{v}_z}{\mathrm{d}\tilde{r}}\right|_{\tilde{r}=1}\right)^2 + \left(\tilde{r}\frac{\mathrm{d}}{\mathrm{d}\tilde{r}}\left(\frac{\tilde{v}_\varphi}{\tilde{r}}\right)\right|_{\tilde{r}=1}\right)^2\right)}\right)}. \tag{25}$$

The boundary conditions at the surfaces of the inner and outer tube can be expressed as

$$\tilde{r} = \kappa: \quad \tilde{v}_z = 0; \quad \tilde{v}_\varphi = N_1$$
$$\tilde{r} = 1: \quad \tilde{v}_z = 0; \quad \tilde{v}_\varphi = N_2. \tag{26}$$

The above differential equations are solved numerically, applying a finite difference method. The numerical integration yields the axial and tangential velocity distribution and the friction coefficient.

3.2. *The equation of energy conservation*

For the solution of the energy equation (7) a turbulence model is also required, which combines the turbulent energy flux with the mean values of velocity and temperature. Similar to the eddy viscosity ε_τ in the momentum equation, the eddy diffusivity ε_q

$$\overline{v_r' T'} = \varepsilon_q \frac{\partial T}{\partial r} = \frac{\varepsilon_\tau}{Pr_t}\frac{\partial T}{\partial r} \tag{27}$$

is introduced. With the turbulent Prandtl number according to Kays and Crawford [9]

$$Pr_t^{-1} = \frac{1}{2\,Pr_{t\infty}} + C\frac{\varepsilon_\tau}{\nu}Pr\sqrt{\frac{1}{Pr_{t\infty}}} - \left(C\frac{\varepsilon_\tau}{\nu}Pr\right)^2\left(1-\exp\left(-C\frac{\varepsilon_\tau}{\nu}\sqrt{Pr_{t\infty}}\right)^{-1}\right) \tag{28}$$

the energy equation will take the form

$$\tilde{v}_z\frac{\partial T}{\partial z} = \frac{1}{r}\frac{\partial}{\partial r}\left((a+\varepsilon_q)r\frac{\partial T}{\partial r}\right). \tag{29}$$

After introducing the dimensionless temperature

$$\theta = \frac{T-T_0}{\dot{q}_w\frac{2r_2(1-\kappa)}{\lambda}} \tag{30}$$

the energy equation can be written as

$$\frac{Re_z\, Pr}{4(1-\kappa)^2}\tilde{v}_z\frac{\partial\theta}{\partial\tilde{z}} = \frac{1}{\tilde{r}}\frac{\partial}{\partial\tilde{r}}\left(\left(1+\frac{\tilde{\varepsilon}_\tau}{Pr_t}\right)\tilde{r}\frac{\partial\theta}{\partial\tilde{r}}\right). \tag{31}$$

The boundary conditions for a fully developed flow with constant heat flux at the outer tube and an adia-

batic inner tube are

$$\tilde{r} = \kappa: \quad \frac{\partial \theta}{\partial \tilde{r}} = 0$$

$$\tilde{r} = 1: \quad \frac{\partial \theta}{\partial \tilde{r}} = \frac{1}{2(1-\kappa)}$$

$$\int_{\tilde{r}=\kappa}^{1} 0 \tilde{v}_{\tilde{z}} \tilde{r} \, \partial \tilde{r} = \frac{2(1-\kappa)}{Re_z Pr} \tilde{z}. \tag{32}$$

Under these conditions the fluid temperature increases linearly in the axial direction, leading to a constant radial temperature profile for large values of $\tilde{z}$. In this case the energy equation has a solution of the form

$$\theta(\tilde{z}, \tilde{r}) = \Gamma(\tilde{z}) + \Psi(\tilde{r}). \tag{33}$$

With the axial temperature distribution

$$\Gamma(\tilde{z}) = \frac{4\tilde{z}}{Re_z Pr(1+\kappa)} \tag{34}$$

the energy equation (31) can be written as

$$\frac{\tilde{v}_{\tilde{z}}}{1-\kappa-\kappa^2+\kappa^3} = \frac{1}{\tilde{r}} \frac{\partial}{\partial \tilde{r}} \left(\left(1 + \frac{\tilde{\varepsilon}_{\tilde{z}}}{Pr_1} \right) \tilde{r} \frac{\partial \Psi}{\partial \tilde{r}} \right). \tag{35}$$

The numerical solution of this differential equation, utilizing the finite difference method, yields the axial and radial temperature distribution of the fluid in the annulus.

The heat transfer coefficient is determined from the temperature distribution. The Nusselt number is based on the temperature gradient at the outer wall and the local difference between wall temperature and fluid bulk temperature:

$$Nu = \frac{\alpha d_h}{\lambda} = \frac{2(1-\kappa) \left. \frac{\partial \theta}{\partial \tilde{r}} \right|_{\tilde{r}=1}}{\theta_{(\tilde{r}=1)} - \theta_b}. \tag{36}$$

With the temperature gradient at the outer wall from equation (32), equation (36) reduces to

$$Nu = \frac{1}{\theta_{(\tilde{r}=1)} - \theta_b} \tag{37}$$

with a bulk temperature θ_b, which is identical to the temperature $\Gamma(\tilde{z})$ from equation (34) at the axial position $\tilde{z}$.

4. RESULTS AND DISCUSSION

Both in the experimental investigation of the heat transfer in the hydrodynamic and thermal entrance region ($z/d_h \approx 60$) and in the theoretical study of the fully developed flow ($z/d_h \to \infty$), a significant influ-

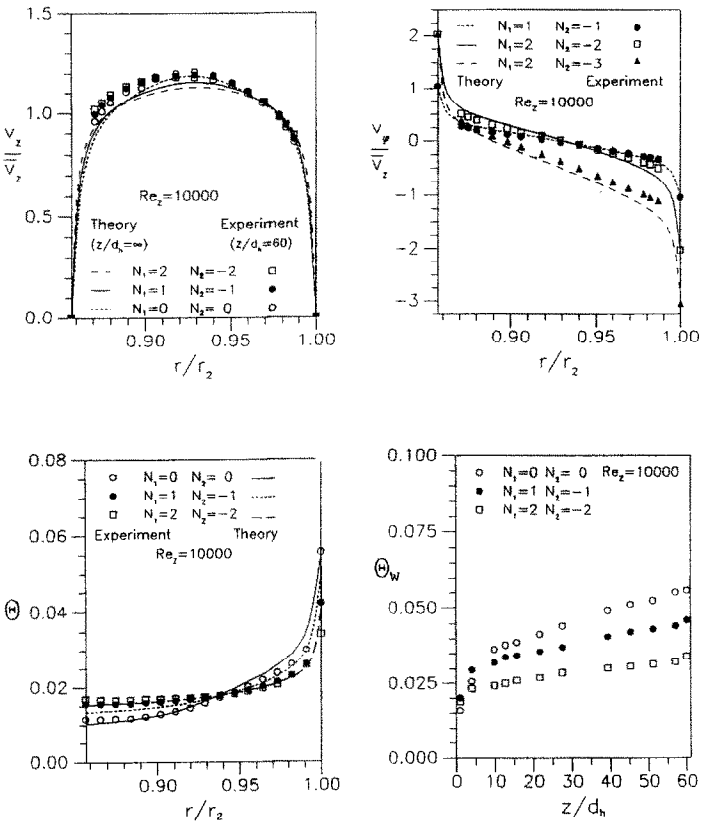

FIG. 2. Velocity and temperature distributions for $Re_z = 10\,000$, with N_1 and N_2 as parameters and the outer wall temperature θ_w.

ence of rotation on heat transfer and fluid flow was observed. The experimental and theoretical results are shown and discussed as follows.

4.1. *Velocity and temperature distribution*

The radial distribution of the fluid velocity and temperature was measured at the end of the test section ($z/d_h \approx 60$) and calculated for fully developed flow. The effects of the rotation rates N_1 and N_2 on the axial and tangential velocity distribution and on the temperature profile are shown representatively in Fig. 2 for the case of counter-rotating tubes. Concerning velocity and temperature profiles of the other co- and counter-rotating configurations under consideration, the reader is referred to ref. [10]. The velocities and temperatures are normalized according to equations (19) and (30).

With increasing rotation rates N_1 and N_2 of the tubes rotating in opposite directions, both velocity profiles approach a more turbulent shape which corresponds to increasing turbulent fluctuations in the fluid. The same effect can be observed at the radial temperature distributions. The curves are aligned in an orderly manner in passing from the uniform heat flux outer boundary to the adiabatic inner boundary. At the outer wall a large temperature decrease can be detected. With increasing rotation in the opposite direction, the inner boundary temperature increases and the temperature at the outer wall decreases. These changes of the radial temperature profiles are caused by enhanced mixing due to flow rotation between counter-rotating tubes. However, it should be emphasized that co-rotating tubes cause a quite different effect on heat transfer. As shown later, the Nusselt number decreases down to its minimum in the case of co-rotating tubes, when both tubes have the same number of revolutions.

Some results of the wall temperature distribution at the outer tube θ_w, are also plotted in Fig. 2. With uniform heating, the wall temperature attains a linear increase at fully developed flow, while the initial region shows a parabolic rise. If both tubes rotate in opposite directions, the wall temperature of the outer tube diminishes over the whole length of the test section. It should be emphasized that the effects shown in Fig. 2 are only valid for counter-rotating tubes. A survey of the different effects of independently rotating tubes on heat transfer is given later.

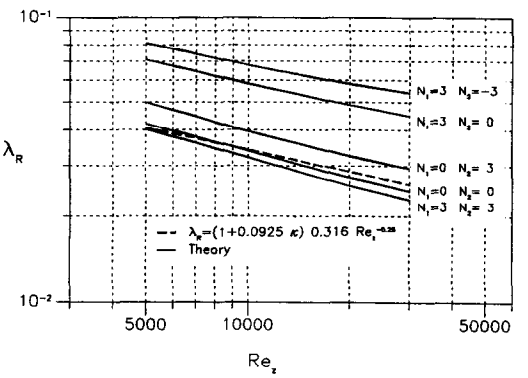

FIG. 3. Calculated friction factor λ_R for fully developed flow as a function of Re_z with N_1 and N_2 as parameters.

4.2. *Friction factor*

In Fig. 3 the friction factor λ_R is plotted against the flow-rate Reynolds number Re_z for various values of the rotation rates N_1 and N_2. With increasing N_1 for $N_2 = 0$, a remarkable rise in λ_R can be observed. An additional counter-rotating outer tube leads to a further small increase of λ_R. On the other hand the friction has its minimum in the case of co-rotating tubes. A mere rotation of the outer tube, with the inner tube at rest ($N_1 = 0$), causes only a small increase of the friction factor. For both rotation rates equal to zero ($N_1 = N_2 = 0$), the friction factor is equal to the value predicted by the Blasius resistance formula, modified by Kakaç *et al.* [11] for an annular flow, according to $\lambda_R = (1+0.0925\kappa)0.316\, Re_z^{-0.25}$.

4.3. *Nusselt numbers*

In Fig. 4 the Nusselt numbers are plotted as a function of the flow-rate Reynolds number Re_z, with the rotational Reynolds numbers $Re_{\varphi 1} = v_{\varphi 1} \cdot d_h/\nu$ and $Re_{\varphi 2} = v_{\varphi 2} \cdot d_h/\nu$, respectively, as parameters, visualizing the influence of mere inner and outer rotation. The measured Nusselt numbers Nu_z are determined

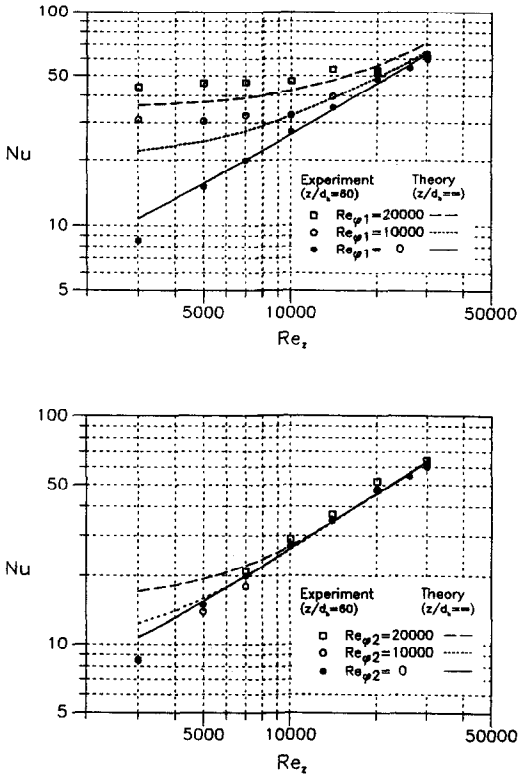

FIG. 4. Nusselt numbers Nu for the cases of mere inner and outer tube rotation, respectively, as a function of Re_z with $Re_{\varphi 1}$ and $Re_{\varphi 2}$ as parameters. Measurements at $z/d_h \approx 60$, theoretical results for $z/d_h = \infty$.

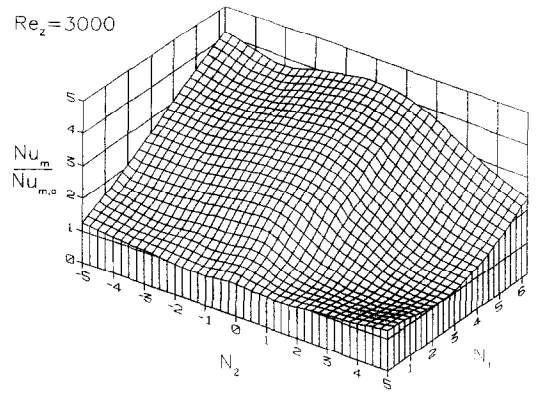

FIG. 5. Three-dimensional representation of the measured mean Nusselt numbers Nu_m as a function of N_1 and N_2 at $Re_z = 3000$.

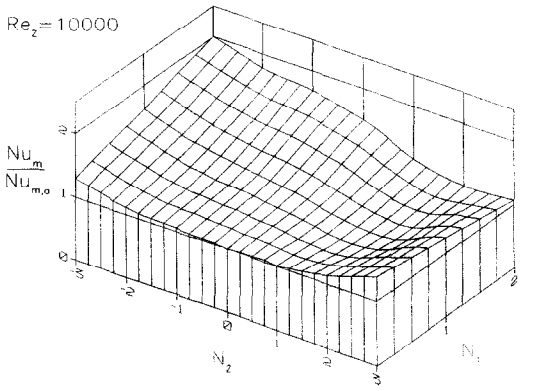

FIG. 7. Three-dimensional representation of the measured mean Nusselt numbers Nu_m as a function of N_1 and N_2 at $Re_z = 10000$.

at $z/d_h \approx 60$, whereas the theoretical values Nu_∞ have been calculated for fully developed flow. It is obvious that the flow is not fully developed at $z/d_h \approx 60$.

With growing rotational Reynolds number of the inner tube, $Re_{\varphi 1}$, and a stationary outer tube, a remarkable increase in the Nusselt number can be observed which is proportional to the rotation rate $N_1 = Re_{\varphi 1}/Re_z$. However, in the case of the outer tube rotating and the inner tube at rest, the Nusselt number does not change significantly, except for very low flow-rate Reynolds numbers and high rotation rates N_2. In this case the calculations reveal an increase of the Nusselt number. Unfortunately no experimental data are available in this region.

In Figs. 5–8 the measured mean Nusselt numbers, Nu_m, at different flow-rate Reynolds numbers are plotted as functions of the two rotation rates N_1 and N_2. In this presentation Nu_m has been divided by the Nusselt number $Nu_{m,0}$, measured for the non-rotating annulus. With stationary outer tube ($N_2 = 0$) and increasing N_1, a remarkable rise in the Nusselt number can be observed. An additional counter-rotating outer tube ($N_2 < 0$) again leads to a small increase of the Nusselt number. On the other hand the heat transfer rates decrease down to their minimum, in the case of co-rotating tubes ($N_2 > 0$), when the tubes have nearly the same number of revolutions. In the region $0.6 < N_1/N_2 < 0.9$, a small decrease of the Nusselt number can be detected. As shown earlier, a sole rotation of the outer tube has only an unimportant influence on the heat transfer rate in the range of Reynolds numbers under consideration. At high flow rate Reynolds numbers, $Re_z = 30000$, measurements could be made only for rotation rates $N < 1$. In this case no significant changes in heat transfer were determined.

In Fig. 9 measured and calculated Nusselt numbers are compared exemplarily for a flow-rate Reynolds number $Re_z = 5000$. The heat transfer rates were measured at the axial position $z/d_h = 60$, while the theoretically determined values are valid for fully developed flow. The experimental results are in close agreement with the theory, although the theoretical analysis mostly underpredicts the experimental findings.

Co-rotating or counter-rotating tubes have a very

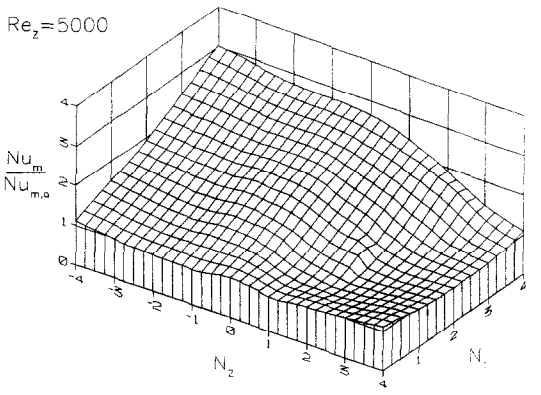

FIG. 6. Three-dimensional representation of the measured mean Nusselt numbers Nu_m as a function of N_1 and N_2 at $Re_z = 5000$.

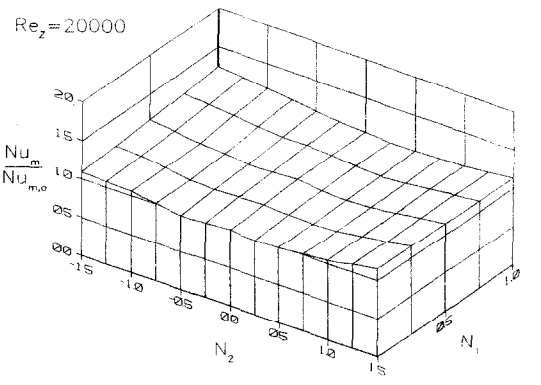

FIG. 8. Three-dimensional representation of the measured mean Nusselt numbers Nu_m as a function of N_1 and N_2 at $Re_z = 20000$.

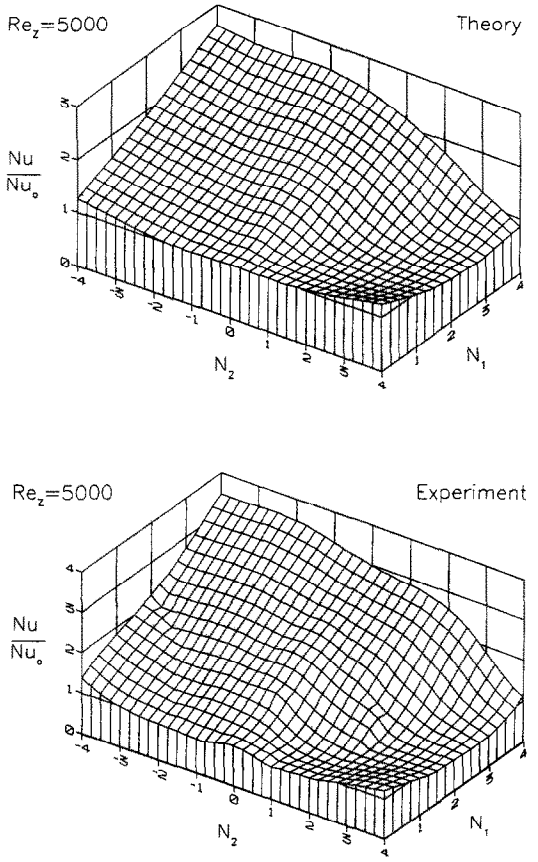

FIG. 9. Comparison of the calculated and measured Nusselt numbers Nu as functions of N_1 and N_2 for $Re_z = 5000$. Theoretical results for $z/d_h = \infty$, measurements at $z/d_h \approx 60$.

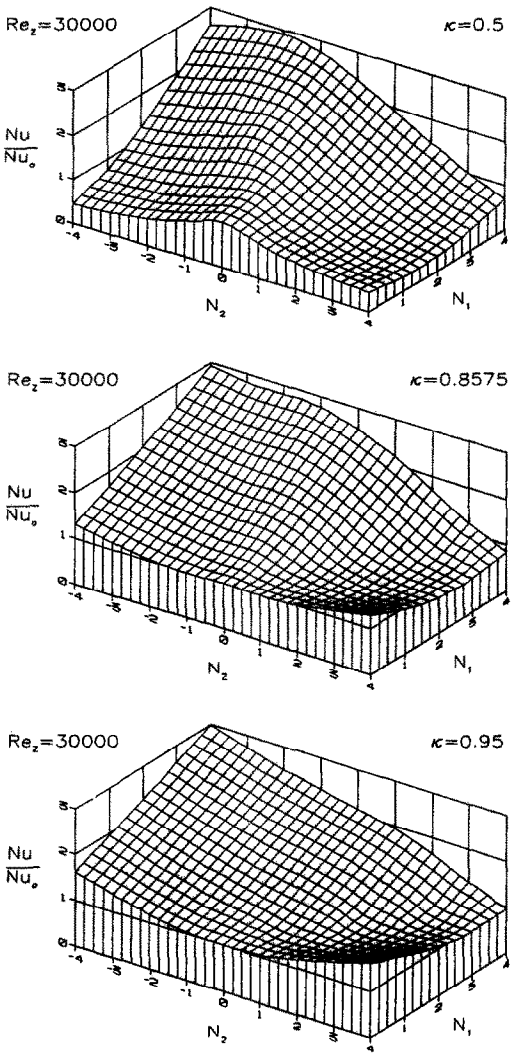

FIG. 10. Calculated Nusselt numbers Nu as functions of N_1 and N_2 at $Re_z = 30\,000$ for different radius ratios κ.

different influence on heat transfer in an annular gap, as revealed above. Heat transfer will decrease with radially growing tangential velocity ($Ri > 0$) and small differences between the rotational velocities of the two tubes. In contrast to this, the heat transfer rates rise with radially decreasing tangential velocity ($Ri < 0$) and very different rotational velocities of the tubes.

4.4. *Influence of radius ratio*

All previous experimental and theoretical results have been gained for a radius ratio $r_1/r_2 = 0.8575$. Because of a considerable experimental complexity the influence of the radius ratio on heat transfer was studied only with the aid of the theoretical model. In Fig. 10 the distributions of the Nusselt number are visualized for different radius ratios $r_1/r_2 = 0.5$, 0.8575 and 0.95. All calculations were performed for a flow-rate Reynolds number of $Re_z = 30\,000$. The influence of the radius ratio is most obvious for the case of mere outer rotation ($N_2 \gtrless 0$; $N_1 = 0$). For low radius ratios ($r_1/r_2 = 0.5$) the Nusselt number decreases with increasing rotating ratio N_2, whereas for high radius ratios ($r_1/r_2 = 0.95$) an increase of Nu with increasing N_2 is predicted. This behaviour can be explained by the opposite effect of the distribution of stabilizing centrifugal forces in the fluid and the increase of shear stress, which stimulates turbulence. In a narrow annulus and for a specified rotation rate, the gradient of the circumferential velocity is larger than in a wide annulus. The larger shear stress $\tau_{r\varphi}$ in the fluid leads to an excitement of turbulence and, therefore, to an increase in heat transfer. On the other hand, the laminarizing effect of the distribution of the stabilizing centrifugal forces, expressed by the Richardson number Ri, gains influence in a wide annulus. Corresponding effects appear for the case of counter-rotating tubes. The region of minimal Nusselt number also changes with the radius ratio. In the absence of further experimental investigations, a comparison between the theoretical results and experimental findings was not possible.

5. CONCLUSIONS

The inner and outer tube rotation in turbulent annular flow produces significant effects on the velocity and temperature fields as well as on heat transfer rate. These effects were studied experimentally in the hydrodynamic and thermal entrance region and theoretically for fully developed turbulent flow in a rotating annulus. In the theoretical study a modified mixing length hypothesis was applied, taking into account the turbulence influence due to streamline curvature.

Both experimental and theoretical investigations reveal a clear enhancement of the Nusselt number with increasing rotation of the inner tube. An additional counter-rotating outer tube leads to a further small increase in heat transfer. On the other hand the Nusselt number decreases with co-rotating tubes down to its minimum, when the outer tube rotates a little faster than the inner tube. The mere rotation of the outer tube, with the inner tube being at rest, has only an unimportant influence on heat transfer for the radius ratio $r_1/r_2 = 0.8575$. However, the theoretical analysis reveals a non-neglectable influence for other radius ratios.

Finally, it has to be pointed out that Taylor vortices could not be detected using the hotwire probe in the range of parameters under consideration.

REFERENCES

1. G. I. Taylor, Stability of a viscous liquid contained between two rotating cylinders, *Phil. Trans R. Soc. Lond.* **A223**, 289–343 (1923).
2. S. Chandrasekhar, The stability of spiral flow between rotating cylinders, *Proc. R. Soc. Lond.* **A265**, 188–196 (1961).
3. J. Kaye and E. C. Elgar, Modes of adiabatic and diabatic fluid flow in an annulus with an inner rotating cylinder, *J. Heat Transfer* **80**, 753–765 (1958).
4. Z. H. Gu and T. Z. Fahidy, Visualization of flow patterns in axial flow between horizontal coaxial rotating cylinders, *Can. J. Chem. Engng* **63**, 14–21 (1985).
5. T. M. Kuzay, Turbulent heat and momentum transfer studies, Ph.D. Thesis, University of Minnesota (1973).
6. M. L. Koosinlin, B. E. Launder and B. I. Sharma, Prediction of momentum, heat and mass transfer in swirling, turbulent boundary layers, *J. Heat Transfer* **96**, 204–209 (1974).
7. P. Bradshaw, Effects of streamline curvature on turbulent flow, AGARDograph No. 169 (1973).
8. H. Schlichting, *Grenzschicht-Theorie*, Verlag G. Braun, Karlsruhe, 8. Auflage (1982).
9. W. M. Kays and M. E. Crawford, *Convective Heat and Mass Transfer*, 2nd Edn. McGraw-Hill, New York (1980).
10. H. Pfitzer, Konvektiver Wärmetransport im axial durchströmten Ringspalt zwischen rotierenden Hohlwellen, Doctoral Thesis, Technische Hochschule Darmstadt (1991).
11. S. Kakaç, R. K. Shah and W. Aung, *Handbook of Single-phase Convective Heat Transfer*, Wiley, New York (1987).

TRANSFERT THERMIQUE DANS UN ESPACE ANNULAIRE ENTRE DES TUBES TOURNANT INDEPENDAMMENT AVEC ECOULEMENT TURBULENT AXIAL

Résumé—On étudie expérimentalement et analytiquement les effets de la rotation des tubes interne et externe sur l'écoulement turbulent d'un fluide et le transfert de chaleur dans un espace annulaire concentrique. On détermine expérimentalement le flux thermique dans la région d'entrée hydrodynamique et thermique de l'espace annulaire et les profils de vitesse et de température en fin de section d'essai. L'étude analytique est conduite pour l'écoulement et le transfert de chaleur d'un écoulement turbulent pleinement établi en appliquant une théorie modifiée de longueur de mélange. Pour exprimer l'accroissement ou la suppression de la turbulence à cause des forces centrifuges dans le fluide créées par la rotation du tube, la longueur de mélange est modifiée par une fonction du nombre de Richardson. Les résultats théoriques pour l'écoulement pleinement établi sont comparés aux données expérimentales à la position axiale de 60 diamètres hydrauliques en aval de l'entrée.

WÄRMEÜBERTRAGUNG IM RINGSPALT ZWISCHEN UNABHÄNGIG VONEINANDER ROTIERENDEN HOHLWELLEN MIT TURBULENTER AXIALSTRÖMUNG

Zusammenfassung—Der Einfluß der rotierenden Innen- und Außenwelle auf die turbulente Strömung und den Wärmetransport in einem konzentrischen Ringspalt wurde experimentell und analytisch untersucht. Im Experiment wurde der Wärmeübergangskoeffizient im hydrodynamischen und thermischen Einlaufbereich des rotierenden Ringspaltes sowie die Geschwindigkeits- und Temperaturprofile am Ende der Versuchsstrecke bestimmt. Das theoretische Modell wurde mit Hilfe eines modifizierten Mischungswegmodelles für die Strömung und den Wärmeübergang einer voll ausgebildeten turbulenten Strömung entwickelt. Die Anfachung oder Unterdrückung der Turbulenz, hervogerufen durch die Fliehkräfte infolge der Rotation, ist in dem Rechenmodell mit einer Modifikation des Mischungsweges durch eine Funktion der Richardsonzahl beschrieben. Die theoretischen Ergebnisse der voll ausgebildeten Strömung wurden mit denjenigen an der Stelle $z/d_h \approx 60$ ermittelten Meßwerten verglichen.

ТЕПЛОПЕРЕНОС В КОЛЬЦЕВОМ КАНАЛЕ МЕЖДУ ТРУБАМИ С ТУРБУЛЕНТНЫМ ОСЕВЫМ ТЕЧЕНИЕМ, ВРАЩАЮЩИМИСЯ НЕЗАВИСИМО ДРУГ ОТ ДРУГА

Аннотация—Экспериментально и аналитически исследуется влияние вращающихся внутренней и наружной труб на турбулентное течение жидкости и теплоперенос в концентрическом кольцевом канале. При экспериментальных исследованиях определяются скорость теплопереноса на гидродинамическим и тепловом входном участке вращающегося канала, а также профили скоростей и температур на границе тестового участка. С использованием модифицированной теории длины смешения аналитически исследуются течение и теплоперенос при полностью развитом турбулентном течении во вращающемся кольцевом канале. Для учета увеличения или подавления турбулентности за счет центробежных сил в жидкости, вызываемых вращением трубы, длина смешения модифицировалась с помощью функции числа Ричардсона. Сравниваются теоретические результаты и экспериментальные данные для полностью развитого течения на расстоянии вниз по течению, соответствующего 60 гидравлическим диаметрам.